**Atmospheric
Chemistry
and Physics**

Heterogeneous chemistry of monocarboxylic acids on α-Al$_2$O$_3$ at different relative humidities

S. R. Tong, L. Y. Wu, M. F. Ge, W. G. Wang, and Z. F. Pu

Beijing National Laboratory for Molecular Sciences (BNLMS), State Key Laboratory for Structural Chemistry of Unstable and Stable Species,Institute of Chemistry, Chinese Academy of Sciences, 100190, Beijing, China

Abstract. A study of the atmospheric heterogeneous reactions of formic acid, acetic acid, and propionic acid on α-Al$_2$O$_3$ was performed at ambient condition by using a diffuse reflectance infrared Fourier transform spectroscopy (DRIFTS) reactor. From the analysis of the spectral features, observations of carboxylates formation provide strong evidence for an efficient reactive uptake process. Comparison of the calculated and experimental vibrational frequencies of adsorbed carboxylates establishes the bridging coordinated structures on the surface. The uptake coefficients of formic acid, acetic acid, and propionic acid on α-Al$_2$O$_3$ particles are $(2.07\pm0.26)\times10^{-3}$ or $(2.37\pm0.30)\times10^{-7}$, $(5.00\pm0.69)\times10^{-3}$ or $(5.99\pm0.78)\times10^{-7}$, and $(3.04\pm0.63)\times10^{-3}$ or $(3.03\pm0.52)\times10^{-7}$, respectively (using geometric or BET surface area). Furthermore, the effect of varying relative humidity (RH) on these heterogeneous reactions was studied. The uptake coefficients of monocarboxylic acids on α-Al$_2$O$_3$ particles increase initially (RH<20%) and then decrease with the increased RH (RH>20%) which was due to the effect of water on carboxylic acid solvation, particle surface hydroxylation, and competition for reactive sites. On the basis of the results of experimental simulation, the mechanism of heterogeneous reaction of α-Al$_2$O$_3$ with carboxylic acids at ambient RH was discussed. The loss of atmospheric monocarboxylic acids due to reactive uptake on available mineral dust particles may be competitive with homogeneous loss pathways, especially in dusty urban and desertified environments.

1 Introduction

About 33% of the earth's land surface is arid and a potential source region for atmospheric mineral aerosol (Tegen and Fung, 1994). Mineral aerosol is a general expression for fine particles of crustal origin that is generated by wind erosion. It can be uplifted into the atmosphere by strong surface winds that travel behind cold frontal systems (Carmichael et al., 1996). Currently, annual dust emissions are estimated in the range of 1000–3000 Tg/year (Li et al., 1996; Prospero, 1999). Particles smaller than 10 μm have atmospheric lifetimes of weeks (Propero, 1999). Mineral aerosol may be transported over thousands of kilometers (Duce et al., 1980; Savoie and Prospero, 1982) and are therefore found far away from their sources resulting in a global distribution of this kind of atmospheric aerosols (Husar et al., 2001). The impact of mineral dust particles on the Earth's atmosphere is manifold. They can absorb and scatter solar and terrestrial radiation and they are of suitability as cloud condensation nuclei (Cziczo et al., 2004). Moreover, recent modeling studies (Dentener et al, 1996; Zhang et al., 1994) have predicted that mineral aerosol could also have a significant influence on atmospheric chemistry by promoting heterogeneous reactions. There is also strong experimental evidence that indicates an important role of mineral dust in modifying atmospheric trace gas distributions. The role of heterogeneous reactions on particulate matter present in the Earth's atmosphere remains an important subject in tropospheric chemistry. Laboratory studies can be quantitatively assessed in atmospheric chemistry models.

Carboxylic acids are one class of oxygenated organic compounds (OVOCs). They arise from biomass and fuel burning (Kawamura et al., 1985; Talbot et al., 1987) and have received increasing attention in the literature in the past

Correspondence to: M. F. Ge
(gemaofa@iccas.ac.cn)

decade. They are a large fraction (25%) of the nonmethane hydrocarbon loading and are prevalent in both urban and remote atmospheres (Chebbi and Carlier, 1996; Khare and Kumari, 1999). Carboxylic acids are responsible for a significant portion of the free acidity in rainwater: up to 35% in North America (Keene and Galloway, 1984) and up to 64% in more remote regions (Keene et al., 1983). Formic acid is the most prevalent carboxylic acid in the gas phase, followed by acetic acid, which is also very abundant in the troposphere with reported concentrations from 0.05–16 ppbv gas-phase (Chebbi and Carlier, 1996). In some regions, the mixing ratio of formic acid can exceed those of HNO_3 and HCl (Nolte et al., 1997). The level of propanoic acid is lower but still significant, in the range 300–700 ppt (Nolte et al., 1999; Satsumabayashi et al., 1989). These oxygenated organic molecules influence the oxidative capacity of the atmosphere through interaction with photochemical HO_x and NO_x cycles, which, in turn, regulate tropospheric O_3 production (Finlayson-Pitts and Pitts, 1997; Kley, 1997); they are also believed to be an important sink for OH radicals in cloudwater, and, as such, they influence oxidation of other important atmospheric species such as SO_2 (Jacob, 1986). In fact, HO_x production from the photolysis of acetone, peroxides, and carboxylic acids, can be more important than HO_x production form the reaction of $O(^1D)$ with H_2O in the upper troposphere (Jacob, 1986; Wennberg et al., 1998). Moreover, the carboxylic acids are more polar and more surface active as they contain both a double-bonded oxygen and a single-bonded oxygen. However, atmospheric sources and sinks of carboxylic acids are not yet well-known, and their concentrations are not well reproduced in most models (von Kuhlmann et al., 2003). Therefore, it is important to understand the processes that control the gas-phase concentrations of these molecules.

Carboxylic acids in the atmosphere have been correlated with mineral aerosol in field studies. During the Atlanta SuperSite Project, Lee and co-workers (2002) analyzed 380 000 spectra of single aerosol particles in the 0.35–2.5 µm size range using laser mass spectrometry instrument. Approximately 40% of the analyzed particles contained fragments associated with organic acids, such as formic and acetic acid. Another study by Russell et al. (2002) using single particle X-ray spectroscopy has observed correlations between large calcium containing particles and fragments indicative of carboxylic acids. Carboxylic acids can increase both the rate of dissolution and solubility of minerals similar to the inorganic acids. Thus, naturally occurring organic acids in dust can affect kinetics and thermodynamics of weathering and diagenesis (Kubicki et al., 1997). Chelation reactions between organic acids and cations in aerosols can drive dissolution of the fine-grained particles comprising the aerosol and enhance the stability of ions in cloud droplets (Ere et al., 1993).

Despite the results of field observations, few studies have been devoted to the heterogeneous chemistry of organic acids with various types of minerals. Most of them have been done at low pressure. In the previous studies, the heterogeneous uptake kinetics of acetic acid on Fe_2O_3, Al_2O_3, and SiO_2 (Carlos-Cuellar et al., 2003) and formic acid on $CaCO_3$ (Al-Hosney et al., 2005) have been measured with a Knudsen cell reactor. Al-Hosney et al. (2005) observed that under humidified conditions, adsorbed water on the surface of the particles participates in the surface reactivity of the particles, enhancing the uptake kinetics as well as the extent of this heterogeneous reaction and opening up several new reaction pathways. Hatch et al. (2007) investigated the heterogeneous uptake of the C_1 to C_4 organic acids on a swelling clay mineral under typical upper tropospheric temperatures and atmospherically relevant RH values. Prince et al. (2008) investigated heterogeneous reaction between calcite aerosol with both nitric and acetic acids in the presence of water vapor which indicated that calcium rich mineral dust may be an important sink for simple organic acids.

Based on the previous studies for mineral dust, the organic acid uptake is sufficiently large that dust may be a significant sink for them in the atmosphere. The uptake coefficient can be expected to be larger under higher RH conditions typical of the ambient troposphere. However, large uncertainties remain concerning the analysis of species formed on the surface and the reaction mechanism under ambient conditions. Therefore, the heterogeneous reaction between dust and carboxylic acids should be studied in depth.

Alumina has a defined chemical composition and is widely used as model oxides for the study of trace gases heterogeneous reactions (Hanisch and Crowley, 2001; Sullivan et al., 2005; Usher et al., 2003). In the present study, the uptake of formic acid, acetic acid, and propionic acid on α-Al_2O_3 particles have been investigated at 300 K, 1 atm synthetic air using a diffuse reflectance infrared Fourier transform spectroscopy (DRIFTS) reactor. Quantum chemical calculations were performed in order to better understand the mechanism of these reactions and study the modes of surface coordinate species on molecular level. Furthermore, the effect of various relative humid (RH) on these heterogeneous reactions were studied.

The aim of this work was to reveal some of the kinetics and mechanism of the reaction between alumina and carboxylic acids at ambient condition and to study whether the loss of atmospheric organic acids due to these reactions can be competitive with homogeneous reactions. The DRIFTS reactor has been employed to probe the heterogeneous chemistry on particle surfaces (Finlayson-Pitts, 2000; Vogt and Finlayson-pitts, 1994; Roscoe and Abbatt, 2005; Zhang et al., 2006) and it can be used to measure in situ spectra of the reaction products without interrupting the reaction processes (Finlayson-Pitts, 2000). DRIFTS can provide mechanistic details not available through other methods. Kinetic data can also be obtained (Vogt and Finlayson-Pitts, 1994) as the uptake coefficient by calibrating the infrared absorbance with ion chromatographic analysis of reacted samples. Probing the chemistry and measuring the rates of these reactions

under atmospheric conditions will provide essential information for developing an accurate computer model of our atmosphere. Characterizing heterogeneous reactions in our atmosphere is one of the first steps towards gaining a more complete understanding of the earth-atmosphere system.

2 Experimental

2.1 Sources of powders and gases

Commercially available α-Al$_2$O$_3$ particles purchased from Alfa Aesar (with a stated minimum purity of 99%) were used for the spectroscopic measurements. The Brunauer-Emmett-Teller (BET) surface area of the particles is measured to be 11.9 m^2 g^{-1} (Autosorb-1-MP automatic equipment, Quanta Chrome Instrument Co.). HCOOH (>97%, Alfa Aesar), CH$_3$COOH (>99.7%, Alfa Aesar), and CH$_3$CH$_2$COOH (>99%, Alfa Aesar) were diluted and mixed with N$_2$ (>99.999%, Beijing Tailong Electronics Co., Ltd) before used. O$_2$ (>99.998%, Orient Center Gas Science & Technology Co., Ltd) was used to simulate the ambient air. Distilled water (Barnstead Easypure II D7411, Thermo Scientific) was degassed prior to use.

2.2 Measurement

Infrared spectra were recorded in the spectral range from 4000 to 650 cm^{-1} with a Nicolet FTIR Spectrometer 6700 equipped with a liquid-nitrogen-cooled narrow band mercury-cadmium-telluride (MCT) detector and DRIFTS optics (Model CHC-CHA-3, Harrick Scientific Corp.). The flow cell in DRIFTS optics has been described in detail elsewhere (Li et al., 2006). The spectra were recorded at a resolution of 4 cm^{-1}, and 100 scans were usually averaged for each spectrum corresponding to a time resolution of 40 s. All the spectral data were automatically collected by Series program in OMINC software in the experimental time. Simultaneously, the integrated absorbance of selected spectral features are obtained.

To obtain reproducible packing of the DRIFTS sampling cup, the powder (60 mg) was pressed into the cup (10 mm diameter, 0.5 mm depth). The sample could be heated and the temperature of the sample cup could be measured by a thermocouple located directly underneath. The outer walls of the reaction chamber were maintained at room temperature by circulating cooled water through a jacked surrounding the cell.

The gas supply system was composed of four inlet lines. The first line supplied diluted organic acids; the second line provided O$_2$; the third line supplied water vapor mixed in nitrogen gas, and the fourth line provided N$_2$. All gases were mixed together before entering the reactor chamber, resulting in a total flow of 400 sccm synthetic air (21% O$_2$ and 79% N$_2$). N$_2$ and O$_2$ were dehumidified by silica gel and molecular sieve before flowing into the system, and the RH was less

than 1% which was called dry condition. The organic acids were diluted by N$_2$ in a glass bottle and the partial pressures were monitored by absolute pressure transducer (MKS 627B range 0 to 1000 torr). Mass flow controllers (Beijing Sevenstar electronics Co., LTD) were used to adjust the flux of diluted organic acids and N$_2$ to an expected concentration. The active gas flow was forced through the powder. Average residence time of gases inside the DRIFTS cell was approximately 2.5 s. A typical experiment lasted 180 min. The DRIFTS cell is connected with other parts through Teflon tube.

To investigate the adsorption behavior of water on the particles, the infrared spectra and adsorptive isothermal curves of water and carboxylic acids on α-Al$_2$O$_3$ were measured using DRIFTS. Pretreated samples were exposed to humid air with different RH at 300 K for 20 min to establish adsorption equilibrium. The infrared spectra at equilibrium were collected.

The integrated absorption bands of the products were calibrated absolutely by analyzing the sample by ion chromatography after reaction. The reacted particles were sonicated for 20 min in 1.5 mL of distilled water. The filtered solution was analyzed using a Dionex ICS 900 system, which was equipped with a Dionex AS 14A analytical column and a conductivity detector (DS5). The number of carboxylate ions found in the samples was linearly correlated to the integrated absorbance of the corresponding absorption bands. Using this calibration the formation rate of carboxylate ions and thus the uptake coefficients for products formation on α-Al$_2$O$_3$ could be calculated.

2.3 Theoretical calculation

IR bands, and adsorption energies of the surface carboxylate species on α-Al$_2$O$_3$ were calculated using the Gaussian 03 program package (Frisch et al., 2003). To calculate the vibrational frequencies of the carboxylate ions, tetrahedrally coordinated binuclear cluster models of the formula [Al$_2$(OH$_4$)(μ–OH)(RCOO)] (Baltrusaitis et al., 2007; Grassian, 2008) were used. The structure parameter of the coordinated carboxylate species were optimized with DFT method. The Becke-three-parameter Lee-Yang-Parr functional (B3LYP) with the 6-311++G(3df,3pd) basis set was used throughout this work. A vibrational analysis was performed for the optimized structure to compare with the IR spectra obtained experimentally. The structure, vibrational frequencies and intensities for the calculated models by the Gaussian 03 program were analyzed by the Gaussview 3.07 program package. Generally, theoretical harmonic frequencies overestimate experimental values due to incomplete descriptions of electron correlations and neglecting mechanical anharmonicity. To compensate for this problem, a uniform scaling factor of 0.9726 was used on calculated frequencies obtained at the B3LYP level of theory (Halls et al., 2001). As reported by Irikura et al. (2005), the scaling factor depends
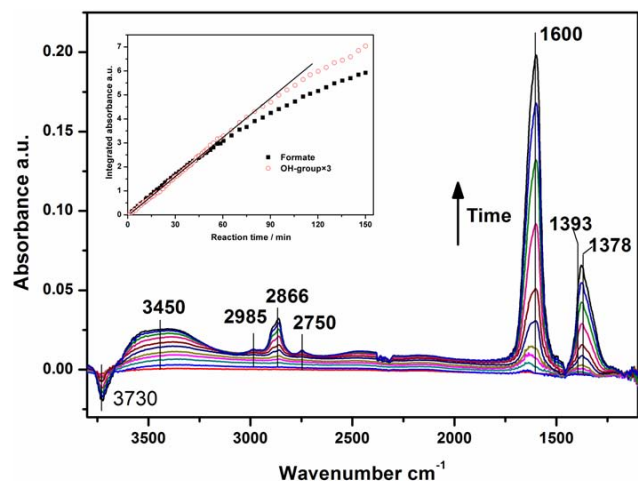
Fig. 1. Absorption spectra recorded during the reaction of HCOOH ([HCOOH]$_0$ = 1.23×10^{14} molecules cm^{-3}) on α-Al$_2$O$_3$ particles. The inset shows the temporal evolution of the integrated absorbance of the formate absorption band (1250–1450 cm^{-1}) and the OH absorption band (3600–3800 cm^{-1}).
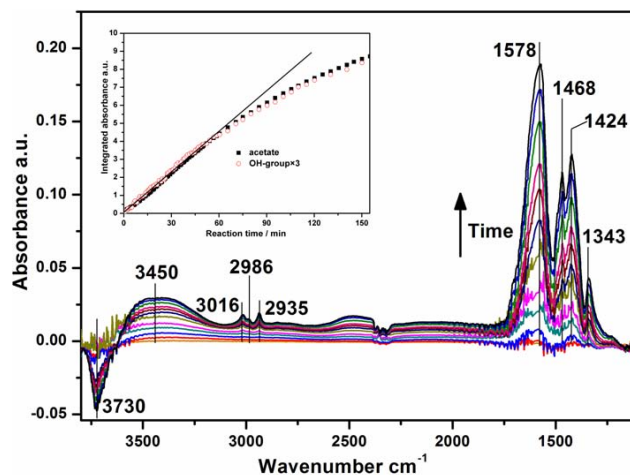

Fig. 2. Absorption spectra recorded during the reaction of CH$_3$COOH ([CH$_3$COOH]$_0$ = 1.23×10^{14} molecules cm^{-3}) on α-Al$_2$O$_3$ particles. The inset shows the temporal evolution of the integrated absorbance of the acetate absorption band (1330–1510 cm^{-1}) and the OH absorption band (3600–3800 cm^{-1}).

only weakly on the basis set, thus it can be used for the majority of basis sets under the same level of theory as used in these calculations.

3   Results and discussion

3.1   Observed products

Prior to initiation of the heterogeneous reactions, the reaction chamber was evacuated and then flushed with carrier gas while the sample was kept at 573 K for 3 h by dry synthetic air before the experiment was started. This treatment gives stable conditions and also removes adsorbed species such as adsorbed water, from the surface (Koretsky et al., 1997; Morterra and Magnacca, 1996; Börensen et al., 2000). After the system was cooled to 300 K, a background spectrum of the unreacted particles was recorded. Spectra were collected as difference spectra with the unreacted particles as the background and surface products were shown as positive bands while losses of surface species were shown as negative bands. Fundamental vibrations of α-Al$_2$O$_3$ are localized in the low frequency region around 1100 cm^{-1} of the IR spectrum. Therefore, the spectral range extending from 1200–3900 cm^{-1} was selected for all the spectra below.

Figures 1–3 show DRIFTS spectra (absorbance units) of three carboxylic acids adsorbed on α-Al$_2$O$_3$ at room temperature under dry conditions (RH<1%). The spectra were recorded in the presence of the gas phase at a concentration of 1.23×10^{14} molecules cm^{-3}. Assignments of the absorbance bands were facilitated by examination of spectra in the literature that involved the reactions of carboxylic acids on solids.
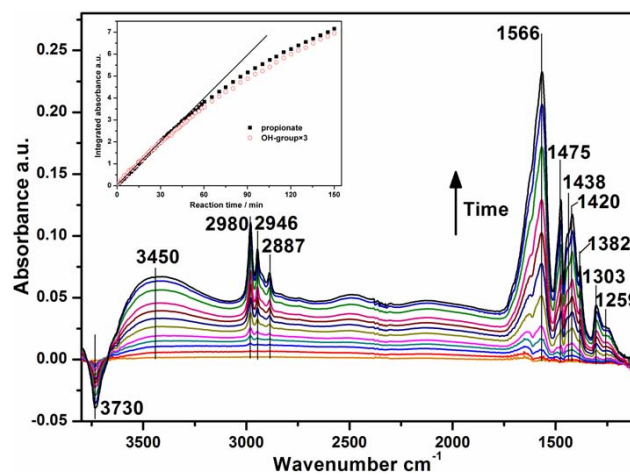

Fig. 3. Absorption spectra recorded during the reaction of CH$_3$CH$_2$COOH ([CH$_3$CH$_2$COOH]$_0$ = 1.23×10^{14} molecules cm^{-3}) on α-Al$_2$O$_3$ particles. The inset shows the temporal evolution of the integrated absorbance of the propionate absorption band (1360–1510 cm^{-1}) and the OH absorption band (3600–3800 cm^{-1}).

When formic acid was introduced to the flow system several absorption bands were observed 1600 cm^{-1}, 1378 cm^{-1}, 2866 cm^{-1}, a broad band around 3450 cm^{-1}, a negative band at 3730 cm^{-1}. A shoulder at 1393 cm^{-1} can also be observed. These results are presented in Table S1. The band at 1378 cm^{-1} and the shoulder at 1393 cm^{-1} was associated with C–H in-plane bend and symmetric stretching mode (ν_s(OCO)), respectively, in line with the assignment on other Al$_2$O$_3$ surfaces (Amenomiya, 1979; Chauvin et al., 1990). The negative band indicates loss of surface species which we

will discuss later. Reaction of the acid on the surface to give the formate anion is suggested by the absence of the C=O stretch mode at $1780\,cm^{-1}$ and the C–OH stretch mode at $\sim 1100\,cm^{-1}$ (Klein, 1973). Instead we see clearly the broad OCO antisymmetric stretch mode (ν_{as}(OCO)) of the formate anion at $1600\,cm^{-1}$ (Table S1).

Adsorption and surface reaction of acetic acid were monitored on α–Al_2O_3 particles. The absence of a peak characteristic of the C=O stretch of acetic acid in the region 1690–$1790\,cm^{-1}$ clearly indicates that the physisorbed acetic acid is inexistent (Bertie and Michaelian, 1982; Pei and Ponec, 1996). Upon adsorption of CH_3COOH on the surface of α–Al_2O_3, several prominent bands are seen to grow. Bands at 1343, 1424, 1468, 1578, 2935, 2986, and $3016\,cm^{-1}$ are shown to increase in intensity as the times of gas phase acetic acid were increased. We assigned the two peaks at $1343\,cm^{-1}$ and $1424\,cm^{-1}$ to C–H deformation (Chen and Bruce, 1995; Walmsley et al., 1981). The peaks of 1578 and $1468\,cm^{-1}$ are correlated to two C–O stretching vibrations of the OCO group of acetate (Dobson and McQuillan, 1999; Gao et al., 2008; Pei and Ponec, 1996). Further confidence in the assignment of the 1468 and $1424\,cm^{-1}$ bands comes from the spectra of CD_3COO^- and CF_3COO^- adsorbates on aluminium oxide (Brown et al., 1979). The $1424\,cm^{-1}$ band is entirely absent from both as would be expected if it is due to a CH_3 mode. Superimposed on ν_{sym}(OCO) is the symmetric methyl bending mode, $\delta_s(CH_3)$, which is located at $1343\,cm^{-1}$. This peak is significantly smaller than the carboxylate stretching modes, but still sharp and distinct. These bands indicate the acetate forms on the surface.

Figure 3 shows the typical time series monitored during the exposure of CH_3CH_2COOH to α–Al_2O_3. In comparison with the vibrational features of the liquid–phase (Jakobsen et al., 1971) and gas-phase CH_3CH_2COOH, the absence of the ν(OH) and ν(C=O) indicates that the physisorbed propionic acid is inexistent. Similar to the vibrational features of HCOOH and CH_3COOH, the product of heterogeneous reaction between propionic acid and α-Al_2O_3 is propionate. The peaks at 1566, 1475 and $1420\,cm^{-1}$ are assigned to ν_{as}(OCO) and ν_s(OCO) of OCO group, respectively. Due to CH_2 and CH_3 group of CH_3CH_2COOH, more bands are appeared at the region in 1200–$1500\,cm^{-1}$. The peaks at 1259, 1303, 1382, 1420, and $1475\,cm^{-1}$ are assigned to the vibrational features of CH_3 and CH_2 groups (Yang et al., 2006), respectively. The assignment of the other bands are shown in Table 1S.

Comparing the three carboxylic acids, we note that the peak (ν_{as} (COO) 1600–$1550\,cm^{-1}$) red shifts by $\sim 15\,cm^{-1}$ for each additional CH_2 unit added to the molecule. Formate is unique, lacking any C-C bond, and has a much higher ν_{as} than the other compounds. The ν_{as} frequency decreases as the number of carbon atoms increases from 1–3, finally reaching a minimum at $1566\,cm^{-1}$ for propionate. Spectral features indicative of carboxylates are present from the spectra (Max and Chapados, 2004).

For the heterogeneous reactions of three carboxylic acids, an interesting observation is the decrease in absorption of a peak centered at $3730\,cm^{-1}$. This band has been described before (Börensen et al., 2000; Morerra and Magnacca, 1996) and is attributed to a loss of OH surface species. Negative features of this band indicate either loss of hydroxyl groups from the surface or that the hydroxyl groups are involved in hydrogen bonding. These groups may present reactive sites for adsorption of organic acids and are ubiquitous on alumina which can be replaced by nucleophilic reagents. The OH band at around 3690–$3800\,cm^{-1}$ was identified as being coordinated to an tetrahedral Al site and termed the I–a group by Knözinger and Ratnasamy (1978), and it is generally ascribed to the basic hydroxyl group (Morterra and Magnacca, 1996). Datka et al. (1994) reported that higher frequency OH bands (above $3700\,cm^{-1}$) were consumed during carboxylate formation on γ–Al_2O_3 and concluded that the formation of carboxylate is related to the basic hydroxyl groups. On the other hand, Boehm (1971) studied the adsorption of NO_2 on η–Al_2O_3 and suggested that formation of nitrate is related to the basic OH groups. From the above mentioned, it is suggested that the basic OH group is reactive and removed or exchanged upon formation of carboxylates, resulting in coordination of carboxylates on the Al–O site with an anion vacancy.

The band observed at $1640\,cm^{-1}$ at initial stage and the broad band around $3450\,cm^{-1}$ were assigned as the frequency of H_2O which was the byproduct of the heterogeneous reaction. This phenomena is similar to water vapor adsorbed on dry α–Al_2O_3 surface (Fig. S1). When water from the vapor phase condenses onto an inert surface, the asymmetric and symmetric stretching modes at 3756 and $3657\,cm^{-1}$, respectively, collapse into a broad, irregularly shaped band with a principal maximum near $3400\,cm^{-1}$ with a full width at half height of $400\,cm^{-1}$ in the infrared spectrum. This band is primarily associated with O-H stretching modes with some contribution from the first overtone of the H-O-H bending mode (Downing and Williams, 1975; Luck, 1974; Eisenberg and Kauzmann, 1969; Goodman et al., 2000). The occurrence of strongly hydrogen bonded water may be explained by the fact that protons react with hydroxyl groups to form adsorbed water during the reaction of the α-Al_2O_3 with organic acids and remains attached to the surface.

3.2 Conformational analysis of carboxylates generated on α–Al_2O_3 surface by DFT calculations

It has been shown that mainly carboxylate species were formed on the α-Al_2O_3 surface. The vibrational frequency at which the OCO band is formed, can give us information about the way it coordinates to the surface. Since the OCO stretching band is most sensitive to its interaction with the metal, the relationship between this frequency and arrangement of the carboxylates on the surface has been studied by
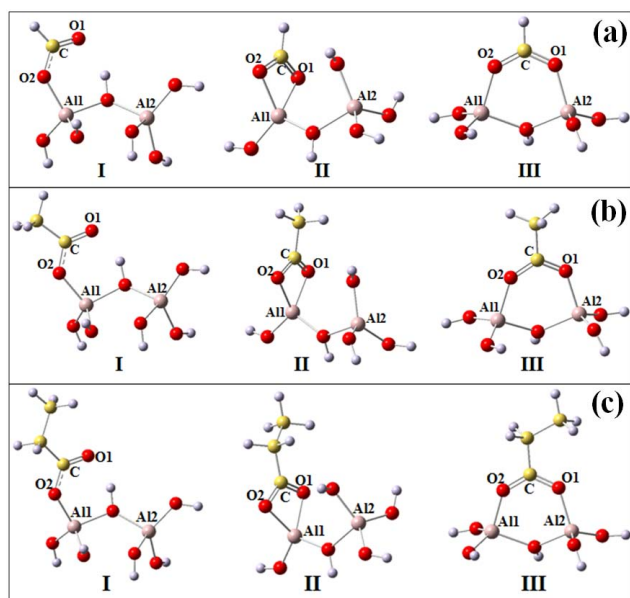
Fig. 4. Optimized structure of the computational models (I–III) for (a) formate, (b) acetate, and (c) propionate species on α-Al$_2$O$_3$ surface. Red circles represent O atoms; yellow circles represent C atoms; pink circles represent Al atoms; Gray circles represent H atoms.

several investigators (Gao et al., 2008; Hedberg et al., 2009; Rachmady and Vannice, 2002). There may exist three coordination modes: a monodentate mode where one carboxylate oxygen is coordinated to a surface Al atom (model I), a bidentate mode involving a deprotonated molecule where the two carboxylate oxygens are bonded to the same Al atom (model II), and a bridging mode similar to above but where the two oxygens of carboxylate are coordinated to two different surface Al atoms (model III) (Alcock et al., 1976; Dobson and McQuillan, 1999; Mehrotra and Bohra, 1983; Popova et al., 2007).

In recent years, in addition to the conventional spectroscopic techniques, quantum chemistry has been applied to state of adsorbed species and the structure of the adsorption sites in gas adsorption on particles (Baltrusaitis et al., 2007; Gao et al., 2008; Grassian, 2008; Yang et al., 2006). To understand the exact structures of adsorbed carboxylates and assignment of carboxylate species on the particles surface clearly, we tried to compare the adsorption energies and frequencies of the IR bands of carboxylates adsorbed on the respective sites with the values evaluated from the calculation method utilizing the DFT method.

Vibrational frequencies were then calculated for adsorbed formate corresponding to different modes of bonding to the surface. The optimized geometry of three different modes for these carboxylic acids are shown in Fig. 4. Only frequencies in 1300–1610 cm^{-1} region are given to investigate the characteristic OCO and C-H vibrations. Tables S2–S4 give the structural parameters including bond lengths and bond

angles, as well as the calculated vibrational frequencies for models I–III.

The calculated vibrational modes ν_{as} (COO) for the models I–III are 1651, 1513, and 1606 cm^{-1}, respectively. In comparison with the same experimental frequency of 1600 cm^{-1}, the calculated frequency of bridging mode with the least error (6 cm^{-1}) is relatively good match of the band 1600 cm^{-1} in the experimental spectrum (Fig. 1). The calculated vibrational modes ν_s (COO) for the calculated models I–III are 1268, 1362, and 1393 cm^{-1}, respectively. For the same experimental frequency of 1393 cm^{-1}, the calculated frequency of bridging mode is good match of this band in the experimental spectrum (Fig. 1). Similarly, the calculated frequency of bridging mode with the least error (5 cm^{-1}) is also good match of δ(CH) with 1378 cm^{-1} band in the experimental spectrum (Fig. 1). Therefore, the spectra of bridging mode simulated by DFT evidently best match the experimental counterparts for the three calculated models.

The calculated ν_{as}(OCO), ν_s(OCO), and δ(CH) vibrational modes of bridging mode acetate are also good matches of the experimental spectrum with the errors -6, 4, and 6 cm^{-1}, respectively. Similarly, the most possible conformation for propionate is bridging mode.

Therefore, the spectra of bridging mode simulated by DFT evidently best match the experimental counterparts for the three carboxylic acids and the substitution of the H atom with the CH$_3$ group and CH$_3$CH$_2$ group does not considerably influence the adsorption mode of the acid.

3.3 Uptake coefficient and kinetics

Combined with ion chromatography, kinetic data can be deduced from the DRIFTS experiments. In the inset in Figs. 1–3, the integrated absorbance of 1250–1450 cm^{-1}, 1360–1510 cm^{-1}, and 1330–1510 cm^{-1} for formate, acetate, and propionate, respectively, formed during the reaction as functions of reaction time are shown. The obvious peaks of ν_{as}(OCO) were not used to avoid the error from the overlapping vibration of water (1640 cm^{-1}). As can be seen from Figs. 1–3, the integrated absorbance initially increases approximately linerly with time. Whereas the linear region of this increase corresponds to a constant formation rate of carboxylate ions on the surface, at reaction times longer than 50 min the integrated absorbance starts to level off indicating that the formation rate slows down. In addition, the absolute values of the integrated absorption band due to surface OH–groups (3600–3800 cm^{-1}) are shown in the inset of Figs. 1–3. For better comparison of the OH peak and surface species, the integrated absorption bands of OH-group were multiplied by a factor three. The intensity of the negative band at 3730 cm^{-1} due to the basic OH group increased with time in a flow of carboxylic acids, which is likely to coincide with an increase of the carboxylate bands. This result suggests again the coordination of carboxylates on the Al–O site.

Table 1. Summary of the reactive uptake coefficients obtained for the uptake of three organic acids on α-Al$_2$O$_3$ particles at $T = 300$ K using DRIFTS measurements.

Organic acid	γ(RCOOH) geometric	γ(RCOOH) BET	References
HCOOH	$(2.07\pm0.26)\times10^{-3}$	$(2.37\pm0.30)\times10^{-7}$	[a]$(3\pm1)\times10^{-3}$, [b]1.7×10^{-5}
CH$_3$COOH	$(5.00\pm0.69)\times10^{-3}$	$(5.99\pm0.78)\times10^{-7}$	[c]$(2\pm1)\times10^{-3}$ [b]1.3×10^{-5}
CH$_3$CH$_2$COOH	$(3.04\pm0.63)\times10^{-3}$	$(3.03\pm0.52)\times10^{-7}$	[b]5.4×10^{-5}

[a] from Al-Hosney et al. (2005). [b] from Hatch et al. (2007). [c] from Carlos-Cuellar et al. (2003).

The amount of carboxylate ions on the sample was determined by ion chromatography in order to quantify the carboxylate ions formation rate $d[\text{RCOO}^-]/dt$ in terms of the reactive uptake coefficient. The formation rate was translated from absorption units s^{-1} to RCOO$^-$ s^{-1} by a conversion factor obtained from a calibration plot. The surface products of the carboxylic acids reaction on α-Al$_2$O$_3$ particles in this study were followed using the integrated absorbance-reaction behavior instead of Kubelka-Munk method which is known to give rise to unacceptable uncertainty levels in quantitative experiments (Samuels et al., 2006). The carboxylate concentrations:

$$(\text{integrated absorbance}) \times f = \{\text{RCOO}^-\} \quad (1)$$

f was the conversion factor, and the calculated values for formate, acetate, and propionate are 2.58×10^{18} ions/int.abs, 2.94×10^{18} ions/int.abs, and 3.13×10^{18} ions/int.abs, respectively. The reactive uptake coefficient (γ) is defined as the rate of carboxylate ions formation on the surface divided by the total number of surface collisions per unit time (Z):

$$\gamma = \frac{d\{\text{RCOO}^-\}/dt}{Z} \quad (2)$$

$$Z = \frac{1}{4} \times A_S \times [\text{RCOOH}] \times \sqrt{\frac{8RT}{\pi M_{\text{RCOOH}}}} \quad (3)$$

Where {RCOO$^-$} is surface concentrations of the carboxylate ions (where { } have been used to distinguish surface concentrations from gas–phase concentrations), [RCOOH] is the gas-phase concentration, A_S is the effective sample surface, R is the gas constant, T is the temperature, and M_{RCOOH} is the molecular weight of carboxylic acids. Two extreme cases of effective sample surface need to be considered (Li et al., 2006; Ullerstam et al., 2002). The uptake coefficients of three carboxylic acids on α-Al$_2$O$_3$ are shown in Table 1, both BET surface area and geometric surface area of the sample are used. For the same heterogeneous reaction, the uptake coefficients can differ by about four orders of magnitude depending on the choice of the effective surface area (geometric

or BET area). If the reaction probability is high, the reactants would have no time to diffuse into the sample before reacting and the effective surface area will be the geometric surface area of the sample. If the reaction probability is low, the reactants may have enough time for diffusion into the entire sample and thus the BET surface area would more appropriately represent the effective area. When carboxylates formed is evenly distributed into the sample, the uptake coefficients obtained using the geometric area will be over-estimated. However, the use of the BET area introduces a correction factor than may be necessary as the BET area is measured using molecular nitrogen as the adsorbent. Since molecular nitrogen is of smaller dimensions than carboxylic acids, the surface area accessible to molecular nitrogen may not be accessible to carboxylic acids. The BET area may overestimate the surface area of the particles and thus underestimate the uptake coefficient (Goodman and Grassian, 2000). Therefore, the uptake coefficients obtained using the geometric and BET surface area as the reactive surface area should be respectively considered as higher and lower limits. The uptake coefficient for formic, acetic, and propionic acids are 2.07×10^{-3}, 5.00×10^{-3}, and 3.04×10^{-3} if the geometric surface area is used and 2.37×10^{-7}, 5.99×10^{-7}, and 3.03×10^{-7} if the BET surface area is applied.

There have been a few studies concerning the uptake of organic acid on surfaces of materials, and most of them used Knudsen Cell reactors (KC). The uptake coefficients were of the order of 10^{-3}–10^{-4} (Al-Hosney et al., 2005; Carlos-Cuellar et al., 2003), which is close to our value using the geometric surface area, but significantly higher than the value obtained with the BET surface area. Ullerstam et al. (2003) studied the uptake coefficients for SO$_2$ in the presence of NO$_2$ using the two different techniques, and found the difference between them are by a factor of around 2×10^4 (BET ratios). One important difference in the uptake coefficients from the two methods is that in the KC experiments an initial uptake coefficient has been determined, whereas reactive uptake coefficients are obtained from the DRIFTS experiments. Therefore, this paper represents the reactive uptake coefficients which are lower than initial uptake coefficients

deduced by KC (Al-Hosney et al., 2005; Carlos-Cuellar et al., 2003). Otherwise, The difference in uptake coefficient from our work compared to coefficients found in the literature is also likely due to a difference in substances and experimental conditions. For instance, Hatch et al. (2007) used Na-montmorillonite clay at 212 K; Al-Hosney et al. (2005) used $CaCO_3$ sample with a BET surface area of $1.4 \, m^2 \, g^{-1}$, and both of their experimental conditions were at lower pressure.

Tables S5-7 summarize the results of experiments carried out with carboxylic acids concentrations ranging from 7.7×10^{12} to 2.46×10^{14}, 7.7×10^{12} to 2.46×10^{14}, and 5.1×10^{12} to 1.64×10^{14} for formic, acetic, and propionic acid, respectively. The rates, R, shown in Tables S5–S7 are calculated from the linear initial rate of formation of carboxylates. Equation (2) shows that the uptake coefficient of unreacted surface is expected to be inversely dependent on the reactant concentration in the case of zero-order kinetics and independent on concentration under first-order conditions. In Fig. 5, the formation rate derived from the linear temporal increase of the integrated absorbance of experiments performed at different $RCOOH_{(g)}$ concentration has been plotted against the corresponding RCOOH concentration on a double-logarithmic scale. All the solid lines have a slope near to 1, indicating first-order rate laws for three carboxylic acids uptake on the surface of α-Al_2O_3 and the uptake coefficients are independent of the concentration of the reactive species.

3.4 Role of water in the reaction of carboxylic acids on α-Al_2O_3 particles

Adsorption on mineral surfaces is mostly studied under dry conditions. However, for practical applications, e.g., in environmental chemistry, we are interested in the sorption properties of mineral surfaces for organic compounds under ambient conditions. Hence, it is necessary to consider the influence of humidity because hydrophilic mineral surfaces are partly or completely covered by one or more molecular layers of adsorbed water at ambient humidity. It is becoming increasing clear through laboratory studies that surface adsorbed water plays a role in the heterogeneous chemistry of trace atmospheric gases (Al-Abadleh et al., 2005; Roscoe and Abbatt, 2005). Water is one of the reactants, and should have a fundamental effect on the reaction kinetics. Therefore, the reaction kinetics at different RH were studied using DRIFTS in the presence of the carboxylic acid gas phase at a concentration of 1.23×10^{14} molecules cm^{-3}.

Figure 6 shows the spectra of three carboxylic acids adsorbed on α-Al_2O_3 at humid condition. When carboxylic acids were introduced, the negative bands at $1670 \, cm^{-1}$ and 3000–$3600 \, cm^{-1}$ region indicate water consumed in the formation of hydrated carboxylates or as a reactant. For formic acid, the addition of water vapor to the system caused the peak $2864 \, cm^{-1}$ to shift to $2811 \, cm^{-1}$. This peak is assigned
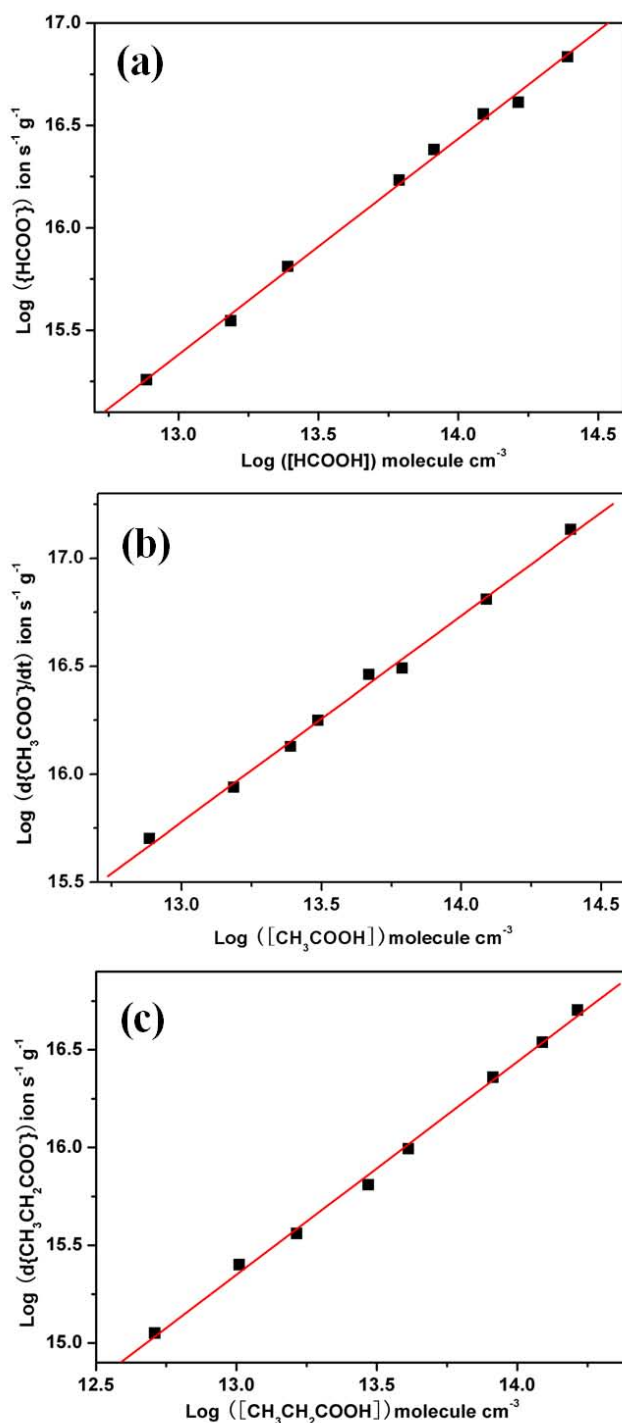

Fig. 5. Bilogarithmic plot of the rate of carboxylates formation as a function of the concentration of **(a)** HCOOH, **(b)** CH_3COOH, and **(c)** CH_3CH_2COOH. The reaction order in HCOOH, CH_3COOH, and CH_3CH_2COOH was determined from linear regression to be $n = 1.05 \pm 0.02$ (RSD = 3.26%), $n = 0.95 \pm 0.03$ (RSD = 3.27%), and $n = 1.09 \pm 0.02$ (RSD = 3.37%), respectively.
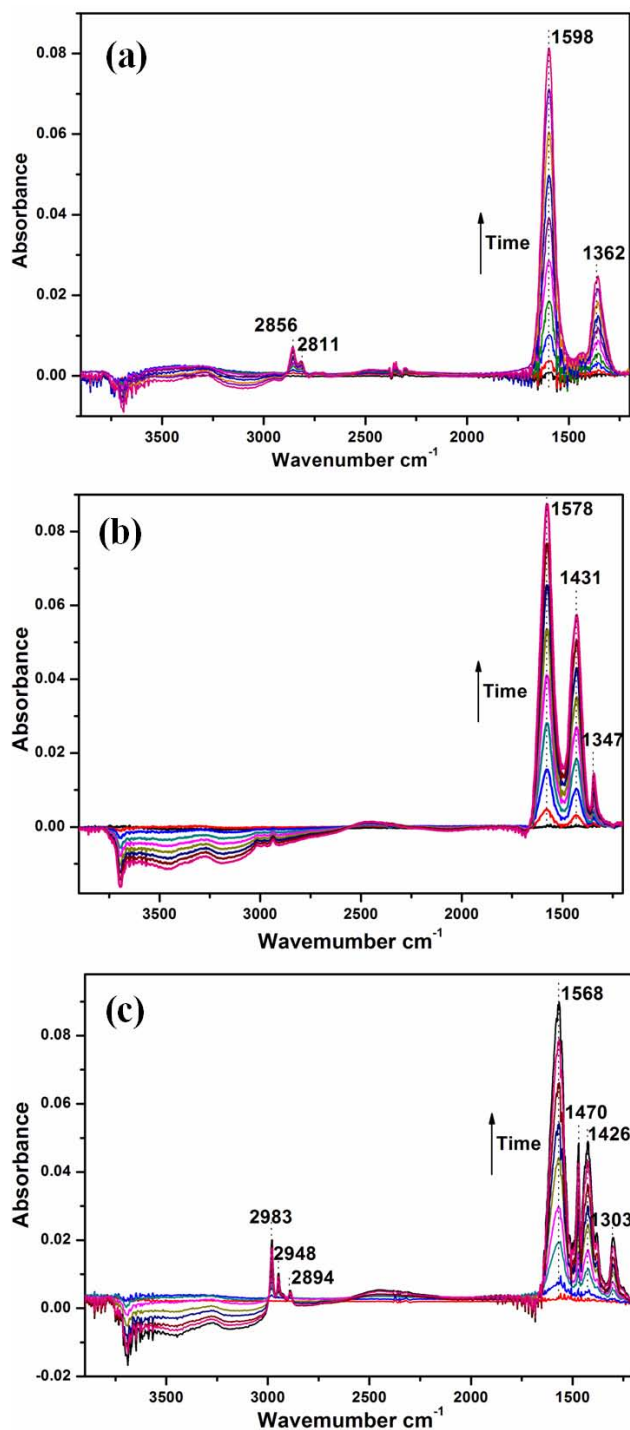
Fig. 6. Absorption spectra recorded during the reaction of **(a)** HCOOH, **(b)** CH_3COOH and **(c)** CH_3CH_2COOH ($[RCOOH]_0 = 1.23 \times 10^{14}$ molecules cm^{-3}) on $\alpha-Al_2O_3$ particles at 30% RH.

to the C-H stretch of formate ion. The C–H band is sensitive to the hydration state of formate. The presence of water red shifts this peak approximately $50\,cm^{-1}$, as observed by both IR and Raman spectroscopy of bulk aqueous HCOONa (Bartholomew and Irish, 1993; Iro and Bernstein, 1956) and VSFS spectroscopy of exposure of ZnO/Zn to wet HCOOH (Hedberg et al., 2009). Thus the peak at $2811\,cm^{-1}$ on the $\alpha-Al_2O_3$ surface is attributed to the hydrated formate. During the $\delta(CH)$ and ν_s (OCO) regions, the appearance of the $1362\,cm^{-1}$ peak also red shifts after exposure in humid which may attribute to the formate ion (Spinner, 1985). Simultaneously, the peak at $2856\,cm^{-1}$, which belongs to surface formate coordinate still exists. Therefore, the oxide coordinated and hydrated formate coexist at wet condition. For acetic and propionic acids adsorbed on $\alpha-Al_2O_3$ particle surface at wet condition, the similar phenomena are observed as that of formic acid. Similarly, for acetic and propionic acids, the bands of $\delta(CH_3)$ and ν_s (OCO) regions also changed at high RH, which may indicate the coexistence of hydrated carboxylate. These spectral changes may suggest that the environment of the carboxylate groups is different after exposure to adsorbed water.

The presence of water has two potential roles in this process: solvation of the carboxylate ion, and hydroxylation of the particles surface. Using crystal truncation rod (CTR) diffraction techniques, Eng et al. (2000) examined the structure of the hydrated $\alpha-Al_2O_3$ (0001) surface. The fully hydrated surface is oxygen-terminated with a contracted aluminum layer underneath and is found to have a structure which is intermediate between $\alpha-Al_2O_3$ and $\gamma-Al(OH)_3$ with hydroxylation occurred. Al-Abadleh and Grassian (2003) also found that water adsorbed on the surface in an ordered fashion with the formation of a stable hydroxide layer at lower RH. Although a rather high initial sticking coefficient of 0.1 has been measured for H_2O on Al_2O_3 at 300 K, the sticking coefficient was found to decrease exponentially with increasing water coverage (Elam et al., 1998). After the surface is fully hydroxylated, additional water can only be physisorbed on the hydroxyl layer on Al_2O_3 (Al-Abadleh and Grassian, 2003; Elam et al., 1998; Goodman et al., 2001; Liu et al., 2009). Because surface -OH is the reactive site for the heterogeneous reaction of carboxylic acids, the formation of surface -OH should promote the reaction while the molecular adsorption of water on surface -OH should suppress this reaction. Theoretically, the uptake coefficients on $\alpha-Al_2O_3$ should increase initially and then decrease with the increased RH. This turning point was observed in our experiment (Fig. 7).

The coverage of adsorbed water on $\alpha-Al_2O_3$ can be quantified by generating adsorption isotherm curves. The three parameter BET equation (Goodman, et al., 2001) was used to obtain a fit to the experimental data (Fig. S1). The relative humidity, corresponding to one monolayers of water adsorbed on $\alpha-Al_2O_3$ surface is calculated to be 19%. This result is similar to other investigations. Studies of water
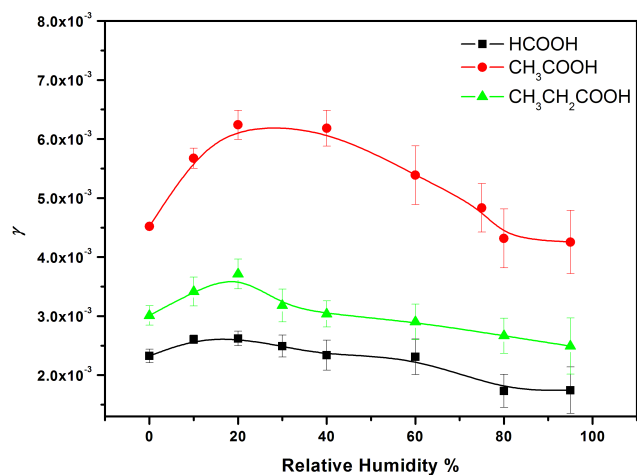
Fig. 7. Uptake coefficients for the reactions of alumina with carboxylic acids as a function of RH.

adsorption versus relative humidity on α-Al_2O_3 powder showed that approximately one monolayer formed at 20% relative humidity, two to three adsorbed water layers formed at 50% relative humidity, and three to four adsorbed water layers formed at 85% relative humidity (Eng et al., 2000; Goodman et al., 2001). It can be also observed from Fig. S1 that there is a negative feature around $3730\,cm^{-1}$. This feature is associated with the loss of OH groups on the surface due to hydrogen bonding to adsorbed water molecules (Al-Abadleh and Grassian, 2003). And there is a small peak at $3690\,cm^{-1}$ in low RH (10%) which may indicate the OH groups formed from water and α-Al_2O_3. Therefore, more -OH were formed which promote the reaction rate below 20% RH. Then competitive adsorption of water and carboxylic acids on surface -OH decrease the reaction rate after multilayer water formed. It should be noted that not all of the surface OH sites were consumed by adsorbed water from our results. There still exists some oxide coordinated carboxylates on the surface. Baltrusaitis et al. (2007) have found that there are adsorbed water islands. Water is not adsorbed according to the hypothetical monolayer, but rather in islands such that some surface adsorption sites are still available for reaction by carboxylic acids.

The result in this paper is a little different from that of heterogeneous reactions between $CaCO_3$ and carboxylic acids (Al-Hosney et al., 2005) at high RH. $CaCO_3$ are reactive soluble particles (Goodman et al., 2001). The heterogeneous reaction of acids on $CaCO_3$ is not limited to the surface, the bulk oxygen atoms participate in the reaction as well as the surface oxygen atoms, this participation is enhanced in the presence of water vapor. Nevertheless, α-Al_2O_3 are reactive insoluble particles. The uptake coefficients of carboxylic acids on α-Al_2O_3 decreased above 20% RH which suggest the bulk oxygen doesn't participate in the reaction and the reactions happen only on the surface. The similar

phenomenon was observed in the study of HNO_3 adsorption on oxide particles at wet condition (Goodman et al., 2000; Goodman et al., 2001).
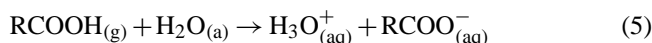
3.5 Mechanism

According to the analysis and the results of the experiments, there is a one step mechanism for the carboxylic acids – α–Al_2O_3 reaction.

$$RCOOH_{(g)} + Al-OH \rightarrow RCOO-Al + H_2O \tag{4}$$

The carboxylate ions and the loss of the proton reacts on the surface with surface hydroxyl groups to form adsorbed water which can be monitored by infrared spectroscopy.

In the presence of adsorbed water, the adsorbed water layer provides another medium for the dissociation reaction and can be written as

$$RCOOH_{(g)} + H_2O_{(a)} \rightarrow H_3O^+_{(aq)} + RCOO^-_{(aq)} \tag{5}$$

4 Conclusion and atmospheric implications

The reaction of three monocarboxylic acids on the surface of α-Al_2O_3 was investigated by DRIFTS. New absorption bands assigned to the formation of carboxylates were observed to grow when the surface was exposed to three carboxylic acids. The vibrational frequency at which the OCO band is formed, can give us information about the way it coordinates to the surface. Comparison of the calculated and experimental vibrational frequencies of adsorbed carboxylates establishes the bridging bidentate corrdinated carboxylate structures. The uptake coefficients of organic acids on α-Al_2O_3 particles increase initially (RH < 20%) and then decrease with the increased RH (RH > 20%), which was due to the effect of water on organic acids solvation, particles surface hydroxylation, and competition on reactive site. The loss of atmospheric organic acids due to reactive uptake on available mineral dust particles may be competitive with homogeneous loss pathways, especially in dusty urban and desertied environment.

The rate of removal of RCOOH by uptake onto mineral dust can be approximated in a simple model. We assume that the lifetime τ for removal of RCOOH by dust is given by

$$\tau = \frac{4}{\gamma \bar{c} A} \tag{6}$$

where A is the dust surface area density in cm^2/cm^3, $\bar{c}$ is the mean molecular speed, and γ is the uptake coefficient. If we assume a conservatively low (i.e., background) dust loading of $5\,\mu g/m^3$ to a high dust loading of $150\,\mu g/m^3$ (Aymoz et al., 2004), we obtained A $\approx 6 \times 10^{-7}\,cm^2/cm^3$ to $1.8 \times 10^{-5}\,cm^2/cm^3$ (assuming the same BET surface area ($11.9\,m^2\,g^{-1}$) as the particles used in this experiment). Our measured uptake coefficient calculated from geometric area

are about 2×10^{-3}, 5×10^{-3}, and 3×10^{-3}, for formic acid, acetic acid, and propionic acid, respectively, which lead to the corresponding lifetimes with respect to processing by dust of 50 min to 25 h, 23 min to 12 h, and 43 min to 21 h, respectively. The main removal mechanism for organic acid is thought to be rainout, as removal rates with respect to photolysis (Chebbim and Carlier, 1996) and reaction with OH (Butkovskaya et al., 2004; Singleton et al., 1989) are low. The lifetimes calculated from our result are shorter than the lifetimes of several days to weeks for removal by reaction with OH. However, using the lower limit of uptake coefficients deduced from BET surface area, the corresponding lifetimes will be so long that can be negligible. These simple calculations show that heterogeneous carboxyliates formation and organic acids remove may be significant, however, further studies of the uptake coefficients are needed.

It can then be concluded from our experimental data and the calculated lifetimes that heterogeneous reactions of carboxylic acids on mineral dust should be included in atmospheric chemistry models if carboxylic acid levels are to be accurately predicted.

Supplementary material related to this article is available online at: http://www.atmos-chem-phys.net/10/7561/2010/ acp-10-7561-2010-supplement.pdf.

Edited by: J. N. Crowley

References

Al-Abadleh, H. A., Al-Hosney, H. A., and Grassian, V. H.: Oxide and carbonate surface composition and surface reactivity, J. Mol. Catal. A-Chem., 228, 47–54, 2005.

Al-Abadleh, H. A. and Grassian, V. H.: FT-IR study of water adsorption on aluminium oxide surfaces, Langmuir, 19, 341–347, 2003.

Al-Hosney, H. A., Carlos-Cuellare, S., Baltrusaitis, J., and Grassian, V. H.: Heterogeneous uptake and reactivity of formic acid on calcium carbonate particles: a Knudsen cell reactor, FTIR and SEM study, Phys. Chem. Chem. Phys., 7, 3587–3595, 2005.

Alcock, N. W., Tracy, V. M., and Waddington, T. C.: Acetates and acetate-complexes. Part 2. Spectroscopic studies, J. Chem. Soc., Dalton Trans., 2243–2246, 1976.

Amenomiya, Y.: Active sites of solid acidic catalysts: III. Infrared study of the water gas conversion reaction on alumina, J. Catal., 57, 64–71, 1979.

Aymoz, G., Jaffrezo, J. –L., Jacob, V., Colomb, A., and George, C.: Evolution of organic and inorganic components of aerosol during a Saharan dust episode observed in the French Alps, Atmos. Chem. Phys., 4, 2499–2512, doi:10.5194/acp-4-2499-2004, 2004.

Baltrusaitis, J., Schuttlefield, J. Jensen, J. H., and Grassian, V. H.: FTIR spectroscopy combined with quantum chemical calculations to investigate adsorbed nitrate on aluminium oxide surfaces in the presence and absence of co-adsorbed water, Phys. Chem. Chem. Phys., 9, 4970–4980, 2007.

Bartholomew, R. J. and Irish, D. E.: Raman spectral studies of solutions at elevated temperatures and pressures. 13. Sodium formate-water, Can. J. Chem., 71, 1728–1733, 1993.

Bertie, J. E. and Michaelian, K. H.: The Raman spectrum of gaseous acetic acid at 21 °C, J. Chem. Phys., 77, 5267–5271, 1982.

Boehm, H. P.: Acidic and basic properties of hydroxylated metal oxide surfaces, Discuss. Faraday Soc., 52, 264–275, 1971.

Börensen, C., Kirchner, U., Scheer, V., Vogt, R., and Zellner, R.: Mechanism and kinetics of the reaction of NO_2 or HNO_3 with alumina as a mineral dust model compound, J. Phys. Chem. A, 104, 5036–5045, 2000.

Brown, N. M. D., Floyd, R. B., and Walmsley, D. G.: Inelastic electron tunnelling spectroscopy (IETS) of carboxylic acids and related systems chemisorbed on plasma-grown aluminium oxide. Part 1.-Formic acid (HCOOH and DCOOD), acetic acid (CH_3COOH, CH_3COOD and CD_3COOD), trifluoroacetic acid, acetic anhydride, acetaldehyde and acetylchloride, J. Chem. Soc., Faraday Trans. 2, 75, 17–31, 1979.

Butkovskaya, N. I., Kukui, A., Pouvesle, N., and Le Bras, G.: Rate constant and mechanism of the reaction of OH radicals with acetic acid in the temperature range of 229-300 K, J. Phys. Chem. A, 108, 7021–7026, 2004.

Carlos-Cuellar, S., Li, P., Christensen, A. P., Krueger, B. J., Burrichter, C., and Grassian, V. H.: Heterogeneous uptake kinetics of volatile organic compounds on oxide surfaces using a Knudsen cell reactor: Adsorption of acetic acid, formaldehyde, and methanol on α-Fe_2O_3, α-Al_2O_3, and SiO_2, J. Phys. Chem. A, 107, 4250–4261, 2003.

Carmichael, G. R., Zhang, Y., Chen, L. L., Hong, M. S., and Ueda, H.: Seasonal variation of aerosol composition at Cheju Island, Korea, Atmos. Environ., 30, 2407–2416, 1996.

Chauvin, C., Saussey, J., Lavalley, J. -C., Idriss, H., Hindermann, J.-P., Kiennemann, A., Chaumette, P., and Courty, P.: Combined infrared spectroscopy, chemical trapping, and thermoprogrammed desorption studies of methanol adsorption and decomposition on $ZnAl_2O_4$ and $Cu/ZnAl_2O_4$ catalysts, J. Catal., 121, 56–69, 1990.

Chebbi, A. and Carlier, P.: Carboxylic acids in the troposphere, occurrence, sources, and sinks: A review, Atmos. Environ., 30, 4233–4249, 1996.

Cziczo, D. J., Murphy, D. M., Hudson, P. K., and Thomson, D. S.: Single particle measurements of the chemical composition of cirrus ice residue during CRYSTAL-FACE, J. Geophys. Res., 109, D04201, doi:10.1029/2003JD004032, 2004.

Datka, J., Sarbak, Z., and Eischens, R. P.: Infrared study of coke on alumina and Zeolite, J. Catal., 145, 544–550, 1994.

Dentener, F. J., Carmichael, G. R., Zhang, Y., Lelieveld, J., and Crutzen, P. J.: Role of mineral aerosol as a reactive surface in the global troposphere, J. Geophys. Res., 101, 22869–22889, 1996.

Dobson, K. D. and McQuillan, A. J.: In situ infrared spectroscopic

analysis of the adsorption of aliphatic carboxylic acids to TiO$_2$, ZrO$_2$, Al$_2$O$_3$, and Ta2O5 from aqueous solutions, Spectrochim. Acta, Part A, 55, 1395–1405, 1999.

Downing, H. D. and Dudley, W.: Optical constants of water in the infrared, J. Geophys. Res., 80, 1656–1661, 1975.

Duce, R. A., Unni, C. K., Ray, B. J., Prospero, J. M., and Merrill, J. T.: Long-range atmospheric transport of soil dust from Asia to the tropical North Pacific: temporal variability, Science, 209, 1522–1524, 1980.

Elam, J. W., Nelson, C. E., Cameron, M. A., Tolbert, M. A., and George, S. M.: Adsorption of H$_2$O on a single-crystal Al$_2$O$_3$ (0001) surface, J. Phys. Chem. B., 102, 7008–7015, 1998.

Eisenberg, D. and Kauzmann, W.: The structure and properties of water, Oxford Univ Press, New York, USA, 1969.

Eng, P. J., Trainor, T. P., Brown Jr., G. E., Waychunas, G. A., Newville, M., Sutton, S. R., and Rivers, M. L.: Structure of the hydrated α-Al$_2$O$_3$ (0001) surface, Science, 288, 1029–1033, 2000.

Erel, Y., Pehkonen, S. O., and Hoffman, M. R.: Redox chemistry of iron in fog and stratus clouds, Clays Clay Miner., 41, 26–37, 1993.

Finlayson-Pitts, B. J.: Chemistry of the Upper and Lower Atmosphere-Theory, Experiments, and Applications, Acdemic Press, New York, USA, 2000.

Finlayson-Pitts, B. and Pitts, J. N., Jr.: Tropospheric air pollution: Ozone, airborne toxics, polycyclic aromatic hydrocarbons, and particles, Science, 276, 1045–1051, 1997.

Frisch, M. J., Trucks, G. W., Schlegel, H. B., Scuseria, G. E., Robb, M. A., Cheeseman, J. R., Montgomery, J. A., Vreven, T., Kudin, K. N., Burant, J. C., Millam, J. M., Iyengar, S., Tomasi, J., Barone, V., Mennucci, B., Cossi, M., Scalmani, G., Rega, N., Petersson, G. A., Nakatsuji, H., Hada, M., Ehara, M., Toyota, K., Fukuda, R., Hasegawa, J., Ishida, M., Nakajima, T., Honda, Y., Kitao, O., Nakai, H., Klene, M., Li, X., Knox, J. E., Hratchian, H. P., Cross, J. B., Adamo, C., Jaramillo, J., Gomperts, R., Stratmann, R. E., Yazyev, O., Austin, A. J., Cammi, R., Pomelli, C., Ochterski, J., Ayala, P. Y., Morokuma, K., Voth, G. A., Salvador, P., Dannenberg, J. J., Zakrzewski, V. G., Dapprich, S., Daniels, A. D., Strain, M. C., Farkas, Ö., Malick, D. K., Rabuck, A. D., Raghavachari, K., Foresman, J. B., Ortiz, J. V., Cui, Q., Baboul, A. G., Clifford, S., Cioslowski, J., Stefanov, B. B., Liu, G., Liashenko, A., Piskorz, P., Komaromi, I., Martin, R. L., Fox, D. J., Keith, T., Al-Laham, M. A., Peng, C. Y., Nanayakkara, A., Challacombe, M., Gill, P. M. W., Johnson, B., Chen, W., Wong, M. W., Andres, J. L., Gonzalez, C., Replogle, E. S., and Pople, J. A., Gaussian 03, revision B.01, Gaussian, Inc., Pittsburgh, PA, USA, 2003.

Gao, H. W., Yan, T. X., Yu, Y. B., and He, H.: DFT and DRIFTS studies on the adsorption of acetate on the Ag/Al$_2$O$_3$ catalyst, J. Phys. Chem. C, 112, 6933–6938, 2008.

Goodman, A. L., Bernard, E. T., and Grassian, V. H.: Spectroscopic study of nitric acid and water adsorption on oxide particles: Enhanced nitric acid uptake kinetics in the presence of adsorbed water, J. Phys. Chem. A, 105, 6443–6457, 2001.

Goodman, A. L., Underwood, G. M., and Grassian, V. H.: A laboratory study of the heterogeneous reaction of nitric acid on calcium carbonate particles, J. Geophys. Res., 105, 29053–29064, 2000.

Grassian, V. H.: Surface science of complex environmental interfaces: Oxide and carbonate surfaces in dynamic equilibrium with

water vapour, Surf. Sci., 602, 2955–2962, 2008.

Halls, M. D., Velkovski, J., and Schlegel, H. B.: Harmonic frequency scaling factors for Hartree-Fock, S-VWN, B-LYP,B3-PW91 and MP2 with the Sadlej pVTZ electric property basis set, Theor. Chem. Acc., 105, 413–421, 2001.

Hanisch, F. and Crowley, J. N.: Heterogeneous reactivity of gaseous nitric acid on Al$_2$O$_3$, CaCO$_3$, and atmospheric dust samples: A Knudsen cell study, J. Phys. Chem. A, 105, 3096–3106, 2001.

Hatch, C. D., Gough, R. V., and Tolbert, M. A.: Heterogeneous uptake of the C$_1$ to C$_4$ organic acids on a swelling clay mineral, Atmos. Chem. Phys., 7, 4445–4458, doi:10.5194/acp-7-4445-2007, 2007.

Hedberg, J., Baldelli, S., and Leygraf, C.: Initial atmospheric corrosion of Zn: Influence of humidity on the adsoption of formic acid studied by vibrational sum frequency spectroscopy, J. Phys. Chem. C, 113, 6169–6173, 2009.

Husar, R. B., Tratt, D. M., Schichtel, B. A., Falke, S. R., Li, F., Jaffe, D., Gassó, S., Gill, T., Laulainen, N. S., Lu, F., Reheis, M. C., Chun, Y., Westphal, D., Holben, B. N., Gueymard, C., Mckendry, I., Kuring, N., Feldman, G. C., McClain, C., Frouin, R. J., Merrill, J., Dubois, D., Vignola, F., Murayama, T., Nickovic, S., Wilson, W. E., Sassen, K., Sugimoto, N., Malm, and W. C.: Asian dust events of April 1998, J. Geophys. Res., 106, 18317–18330, 2001.

Irikura, K. K., Johnso III, R. D., and Kacker, R. N.: Uncertainties in scaling factors for ab Initio vibrational frequencies, J. Phys. Chem. A, 109, 8430–8437, 2005.

Ito, K. and Bernstein, H. J.: The vibrational spectra of the formate, acetate, and oxalate ions, Can. J. Chem., 34, 170–178, 1956.

Jacob, D. J.: Chemistry of OH in remote clouds and its role in the production of formic acid and peroxymonosulfate, J. Geophys. Res., 91, 9807–9826, 1986.

Jakobsen, R. J., Mikawa, Y., Allkins, J. R., and Carlson, G. L.: The vibrational spectra of propanoic acid, J. Mol. Struct., 10, 300–303, 1971.

Kakihana, M. and Akiyama, M.: Vibrational analysis of the propionate ion and its carbon-13 derivatives: Infrared low-temperature specture, normal-coordinate analysis, and local-symmetry valence force field, J. Phys. Chem., 91, 4701–4709, 1987.

Kawamura, K., Ng, L. L., and Kaplan, I. R.: Determination of organic acids (C$_1$-C$_{10}$) in the atmosphere, motor exhausts, and engine oils, Environ. Sci. Technol., 19, 1082–1086, 1985.

Keene, W. C. and Galloway, J. N.: Organic acidity in precipitation of North America, Atmos. Environ., 18, 2491–2497, 1984.

Keene, W. C., Galloway, J. N., and Holden Jr., J. D.,: Measurement of weak organic acidity in precipitation from remote areas of the world, J. Geophys. Res., 88, 5122–5130, 1983.

Khare, Puja, Kumar, N., Kumari, K. M., and Srivastava, S. S.: Atmospheric formic and acetic acids: An overview, Rev. Geophys., 37, 227–248, 1999.

Klein, J. Léger, A., Belin, M., Défourneau, D., and Sangster, M. J. L.: Inelastic-Electron-Tunneling spectroscopy of Metal-Insulator-Metal junctions, Phys. Rev. B, 7, 2336–2348, 1973.

Kley, D.: Tropospheric chemistry and transport, Science, 276, 1043–1044, 1997.

Knözinger, H. and Ratnasamy, P.: Catalytic aluminas: Surface models and characterization of surface sites, Catal. Rev. Sci. Eng., 17, 31–70, 1978.

Koretsky, C. M., Sverjensky, D. A., Salisbury, J. W., and D'Aria,

D. M.: Detection of surface hydroxyl species on quartz, γ-alumina, and feldspars using diffuse reflectance infrared spectroscopy, Geochim. Cosmochim. Acta, 61, 2193–2210, 1997.

Kubicki, J. D., Blake, G. A., and Apitz, S. E.: Molecular orbital calculations for modelling acetate-aluminosilicate adsorption and dissolution reactions, Geochim. Cosmochim. Acta, 61, 1031-1046, 1997.

von Kuhlmann, R., Lawrence, M. G., Crutzen, P. J., and Rasch, P. J.: A model for studies of tropospheric ozone and nonmethane hydrocarbons: Model evaluation of ozone-related species, J. Geophys. Res., 108, 4729, doi:10.1029/2002JD003348, 2003.

Lacaux, J. P., Loemba-Ndembi, J., Lefeivre, B., Cros, B., and Delmas, R.: Biogenic emissions and biomass burning influences on the chemistry of the fogwater and stratiform precipitations in the African equatorial forest, Atmos. Environ., 26 A, 541–551, 1992.

Lee, S.-H., Murphy, D. M., Thomson, D. S., and Middlebrook, A. M.: Chemical components of single particles measured with Particle Analysis by Laser Mass Spectrometry (PALMS) during the Atlanta SuperSite Project: Focus on organic/sulphate, lead, soot, and mineral particles, J. Geophys. Res., 107, 4003, doi:10.1029/2000JD000011, 2002.

Li, L., Chen, Z. M., Zhang, Y. H., Zhu, T., Li, J. L., and Ding, J.: Kinetics and mechanism of heterogeneous oxidation of sulphur dioxide by ozone on surface of calcium caibonate, Atmos. Chem. Phys., 6, 2453–2464, doi:10.5194/acp-6-2453-2006, 2006.

Li, X., Maring, H., Savoie, D., Voss, K., and Prospero, J. M.: Dominance of mineral dust in aerosol light-scattering in the North Atlantic trade winds, Nature, 380, 416–419, 1996.

Liu, Y., Ma, Q., and He, H.: Comparative study of the effect of water on the heterogeneous reactions of carbonyl sulfide on the surface of α-Al_2O_3 and MgO, Atmos. Chem. Phys., 9, 6273–6286, doi:10.5194/acp-9-6273-2009, 2009.

Luck, W. A. P.: Structure of water and aqueous solutions, pp.207-218, Hans richarz Publikationsserv., St. Augustin, Germany, 1974.

Max, J.-J. and Chapados, C.: Infrared spectroscopy of aqueous carboxylic acids: Comparison between different acids and their salts, J. Phys. Chem. A, 108, 3324–3337, 2004.

Mehrotra, R. C. and Bohra, R.: Metal Carboxylates, Academic press, New York, USA, 1983.

Morerra, C. and Magnacca, G.: A case study: Surface chemistry and surface structure of catalytic aluminas, as studied by vibrational spectroscopy of adsorbed species, Catal. Today, 27, 497–532, 1996.

Nakamoto, K.: Infrared and Raman spectra of inorganic and coordination compounds, 5 th ed., Whiley, New York, USA, 1997.

Nolte, C. G., Fraser, M. P., and Cass, G. R.: Gas phase C_2-C_{10} organic acids concentrations in the Los Angeles atmosphere, Environ. Sci. Technol., 33, 540–545, 1999.

Nolte, C. G., Solomon, P. A., Fall, T., Salmon, L. G., and Cass, G. R.: Seasonal and spatial characteristics of formic and acetic acids concentrations in the Southern California atmosphere, Environ. Sci. Technol., 31, 2547–2553, 1997.

Pei, Z.-F. and Ponec, V.: On the intermediates of the acetic acid reactions on oxides: an IR study, Appl. Surf. Sci., 103, 171–182, 1996.

Popova, G. Ya., Andrushkevich, T. V., Chesalov, Y. A., and Parmon, V. N.: Transient response study of the formaldehyde oxidation to formic acid on V-Ti-O catalyst: FTIR and Pulse study, J. Mol.

Catal. A: Chem, 268, 251–256, 2007.

Prince, A. P., Kleiber, P. D., Grassian, V. H., and Young, M. A.: Reactive uptake of acetic acid on calcite and nitric acid reacted calcite aerosol in an environmental reaction chamber, Phys. Chem. Chem. Phys., 10, 142–152, 2008.

Prospero, J. M.: Long-range transport of mineral dust in the global atmosphere: Impact of African dust on the environment of the southeastern United States, Proc. Natl. Acad. Sci. USA, 96, 3396–3403, 1999.

Rachmady, W. and Vannice, M. A.: Acetic acid reduction by H_2 over supported Pt catalysts: A DRIFTS and TPD/TPR study, J. Catal., 207, 317–330, 2002.

Roscoe, J. M. and Abbatt, J. P. D.: Diffuse reflectance FTIR study of the interaction of alumina surfaces with ozone and water vapor, J. Phys. Chem. A, 109, 9028–9034, 2005.

Russell, L. M., Maria, S. F., and Myneni, S. C. B.: Mapping organic coatings on atmospheric particles, Geophys. Res. Lett., 29, 1779, doi:10.1029/2002GL014874, 2002.

Samuels, A. C., Zhu, C. J., Williams, B. R., Ben-David, A., Miles Jr., R. W., and Hulet, M.: Improving the linearity of infrared diffuse reflection spectroscopy data for quantitative analysis: An application in quantifying organiophosphorus contamination in soil, Anal. Chem., 78, 408–415, 2006.

Satsumabayashi, H., Kurita, H., Yokouchi, Y., and Ueda H.: Mono- and di-carboxylic acids under long-range transport of air pollution in central Japan, Tellus, 41B, 219–229, 1989.

Savoie, D. L. and Prospero, J. M.: Particle size distribution of nitrate and sulphate in the marine atmosphere, Geophys. Res. Lett., 9, 1207–1210, 1982.

Singleton, D. L., Paraskevopoulos, G., and Irwin, R. S.: Rates and mechanism of the reactions of hydroxyl radicals with acetic, deuterated acetic, and propionic acids in the gas phase, J. Am. Chem. Soc., 111, 5248–5251, 1989.

Spinner, E.: Futher studies of depolarization ratios in the Raman spectrum of aqueous formate ion, Aust. J. Chem., 38, 47–68, 1985.

Sullivan, R. C., Thornberry, T., and Abbatt, J. P. D.: Ozone decomposition kinetics on alumina: effects of ozone partial pressure, relative humidity and repeated oxidation cycles, Atmos. Chem. Phys., 4, 1301–1310, doi:10.5194/acp-4-1301-2004, 2004.

Talbot, R. W., Beecher, K. M., Harriss, R. C., and Cofer III, W. R.: Atmospheric geochemistry of formic and acetic acids at a mid-latitude temperate site, J. Geophys. Res., 93, 1638–1652, 1987.

Tegen, I. and Fung, I.: Modeling of mineral dust in the atmosphere: Sources, transport, and optical thickness, J. Geophys. Res., 99, 22897–22914, 1994.

Ullerstam, M., Johnson, M. S., Vogt, R., and Ljungström, E.: DRIFTS and Knudsen cell study of the heterogeneous reactivity of SO_2 and NO_2 on mineral dust, Atmos. Chem. Phys., 3, 2043–2051, doi:10.5194/acp-3-2043-2003, 2003.

Ullerstam, M., Vogt, R., Langer, S., and Ljungström, E.: The kinetics and mechanism of SO_2 oxidation by O_3 on mineral dust, Phys. Chem. Chem. Phys., 4, 4694–4699, 2002.

Usher, C. R., Michel, A. E., and Grassian, V. H.: Reactions on mineral dust, Chem. Rev., 103, 4883–4939, 2003.

Vogt, R. and Finlayson-Pitts, B. J.: A Diffuse Reflectance Infrared Fourier Transform Spectroscopic (DRIFTS) study of the surface reaction of NaCl with gaseous NO_2 and HNO_3, J. Phys. Chem., 98, 3747–3755, 1994.

Walmsley, D. G., Nelson, W. J., Brown, N. M. D., de Cheveigné, S., Gauthier, S., Klein, J., and Léger, A.: Evidence from inelastic electron tunnelling spectroscopy for vibrational mode reassignments in simple aliphatic carboxylate ions, Spectochim. Acta, 37A, 1015–1019, 1981.

Wennberg, P. O., Hanisco, T. F., Jaeglé, L., Jacob, D. J., Hintsa, E. J., Lanzendorf, E. J., Yan, B, -D., Meilink, S., Warren, G., and Wynblatt, P.: Water adsorption and surface conductivity measurements on α-alumina substrates, IEEE Trans. Compon., Hybrids, Manuf. Technol., 10, 247–251, 1987.

Yang, X., He, Z. H., Zhou, X. J., Xu, S. H., and Leung, K. T.: Vibrational EELS and DFT study of propionic acid and pyruvic acid on Ni (100): Effects of keto group substitution on roomtemperature adsorption and thermal chemistry, Appl. Surf. Sci., 252, 3647–3657, 2006.

Yuzawa, T., Kubota, J., Onda, K., Wada, A., Domen, K., and Hirose, C.: A TPD and SFG study of propionic acid adsorbed on Ni (110) surface, J. Mol. Struct., 413–414, 307–312, 1997.

Zhang, X. Y., Zhuang, G. S., Chen, J. M., Wang, Y., Wang, X., An, Z. S., and Zhang, P.: Heterogeneous reactions of sulfur dioxide on typical mineral particles, J. Phys. Chem. B, 110, 12588–12596, 2006.

Zhang, Y., Sunwoo, Y., Kotamarthi, V., and Carmichael, G. R.: Photochemical oxidat processes in the presence of dust: An evaluation of the impact of dust on particulate nitrate and ozone formation, J. Appl. Met., 33, 813–824, 1994.